

Report on the Physical Properties and Durability of Fiber-Reinforced Concrete

Reported by ACI Committee 544

Nemkumar Banthia
Chair

Neven Krstulovic-Opara
Secretary

Melvyn A. Galinat
Membership Secretary

Ashraf I. Ahmed	Graham T. Gilbert	Pritpal. S. Mangat*	Venkataswamy Ramakrishnan*
Corina-Maria Aldea*	Vellore S. Gopalaratnam	Peter C. Martinez	Roy H. Reiterman
Madasamy Arockiasamy	Antonio J. Guerra	Bruno Massicotte	Klaus Alexander Rieder*
P. N. Balaguru	Rishi Gupta	James R. McConaghy	Pierre Rossi
Joaquim Oliveira Barros*	Carol D. Hays	Christian Meyer	Surendra P. Shah
Gordon B. Batson*	George C. Hoff	Nicholas C. Mitchell Jr.	Konstantin Sobolev
Vivek S. Bindiganavile	Allen J. Hulshizer	Barzin Mobasher†	Jim D. Speakman Sr.
Peter H. Bischoff	Akm Anwarul Islam	Henry J. Molloy	Chris D. Szychowski
Marvin E. Criswell	John Jones*	Dudley R. Morgan	Peter C. Tatnall
James I. Daniel	Jubum Kim	Antoine E. Naaman*	Houssam A. Toutanji
Xavier Destree	Katherine G. Kuder*	Antonio Nanni	Jean François Trottier*
Ashish Dubey	David A. Lange	Nandakumar Natarajan	George J. Venta
Philip L. Dyer	John S. Lawler*	Jeffrey L. Novak*	Gary L. Vondran*
Gregor D. Fischer	Mark A. Leppert	Mark E. Patton	Robert Wojtysiak
Dean P. Forgeron*	Maria Lopez de Murphy	Max L. Porter	Robert C. Zellers
Sidney Freedman	Clifford N. MacDonald*	John H. Pye	Ronald F. Zollo
Richard J. Frost			

*Subcommittee members who prepared this report.

†Subcommittee Chair.

This document addresses the physical properties and durability of fiber-reinforced concrete (FRC). The effects of fiber reinforcement are evaluated for various physical, short-term, and long-term benefits they impart to the concrete mixture. A variety of test methods, conditions, and properties are reported. The various properties listed, in addition to the wide variety of the choices available in formulating matrix systems, allow performance-based specification of concrete materials using fibers to become a viable option. This document provides a historical basis and an overview of the current knowledge of FRC materials for tailoring new, sustainable, and durable concrete mixtures.

This document is divided into three sections. The first section discusses the physical properties of FRC in terms of electrical, magnetic, and thermal properties. Rheological properties, which affect fiber dispersion and distribution, are discussed using both empirical and quantitative rheology. Mechanisms of

creep and shrinkage and the role of various fiber types in affecting both plastic shrinkage cracking and restrained shrinkage cracking are also addressed. The durability of concrete as affected by the addition of fibers is documented under freezing and thawing, corrosion resistance, and scaling. The durability of FRC systems is also affected as different fibers respond differently to the highly alkaline cementitious microstructure. The durability of alkali-resistant glass and cellulose fibers are studied by an in-depth evaluation of long-term accelerated aging results. Degradation and embrittlement due to alkali attack and bundle effect are discussed. Recent advances for modeling and design of materials with aging characteristics are presented. Literature on the use of FRC materials under aggressive environments, extreme temperatures, and fire is presented. The final sections list a series of applications where the use of FRC has resulted in beneficial durability considerations.

ACI Committee Reports, Guides, Manuals, and Commentaries are intended for guidance in planning, designing, executing, and inspecting construction. This document is intended for the use of individuals who are competent to evaluate the significance and limitations of its content and recommendations and who will accept responsibility for the application of the material it contains. The American Concrete Institute disclaims any and all responsibility for the stated principles. The Institute shall not be liable for any loss or damage arising therefrom.

Reference to this document shall not be made in contract documents. If items found in this document are desired by the Architect/Engineer to be a part of the contract documents, they shall be restated in mandatory language for incorporation by the Architect/Engineer.

Keywords: aging; chloride permeability; corrosion; cracking; creep; diffusion; degradation; ductility; durability; electric properties; embrittlement; fiber-reinforced cement-based materials; fiber-reinforced products; fire resistance; flexural strength; freezing-and-thawing; glass; microcracking; permeability; plastic shrinkage; polypropylene; polyvinyl alcohol; reinforcing materials; rheology; shrinkage cracking; steel; sulfate attack; thermal conductivity; toughness; water permeability; wood pulp.

ACI 544.5R-10 was adopted and published March 2010.

Copyright © 2010, American Concrete Institute.

All rights reserved including rights of reproduction and use in any form or by any means, including the making of copies by any photo process, or by electronic or mechanical device, printed, written, or oral, or recording for sound or visual reproduction or for use in any knowledge or retrieval system or device, unless permission in writing is obtained from the copyright proprietors.

CONTENTS

Chapter 1—Introduction and scope, p. 2

- 1.1—Introduction
- 1.2—Scope

Chapter 2—Notation, definitions, and acronyms, p. 3

- 2.1—Notation
- 2.2—Definitions
- 2.3—Acronyms

Chapter 3—Physical properties of fiber-reinforced concrete (FRC), p. 3

- 3.1—Creep
- 3.2—Shrinkage
- 3.3—Permeability and diffusion
- 3.4—Rheology
- 3.5—Electrical properties
- 3.6—Thermal conductivity

Chapter 4—Durability of FRC, p. 13

- 4.1—Extreme temperature and fire
- 4.2—Freezing and thawing
- 4.3—Degradation and embrittlement due to alkali attack and bundle effect
- 4.4—Weathering and scaling
- 4.5—Corrosion resistance

Chapter 5—Applications and durability-based design, p. 23

- 5.1—Case studies of applications of FRC materials and durability

Chapter 6—References, p. 23

- 6.1—Referenced standards and reports
- 6.2—Cited references

CHAPTER 1—INTRODUCTION AND SCOPE

1.1—Introduction

The use of fibers in concrete to improve pre- and post-cracking behavior has gained popularity. Since 1967, several different fiber types and materials have been successfully used in concrete to improve its physical properties and durability. This is supported by an extensive number of independent research results showing the ability of fibers to improve durability and physical properties of concrete. Regardless of origin, cracking, when induced by chemical, mechanical, or environmental processes, results in deteriorated and less-durable concrete. In addition, the increased permeability caused by cracking can accelerate other deterioration processes such as freezing-and-thawing damage, again resulting in less-durable concrete.

This report addresses the physical properties and durability of FRC that includes fibers in concrete. In this report, many structural systems are evaluated for various physical, short-term, and long-term benefits. These effects of using fibers have been determined using various testing methods. Many needed tests are not described by existing ASTM standards and similar standards due to the diverse nature of test methods, conditions, and properties reported. It would be a daunting task to address every project in an effort to develop correlations across the various test results. This report presents a limited collection of the published research results in relevant area. With the exception of a few characteristic responses such as creep, plastic shrinkage cracking, and long-term aging, this report does not address the mechanical properties in detail. The justification for this treatment is that topics such as mechanical properties and testing methods are addressed by subcommittees. The broader category of physical properties is in context to specific chapters.

There are several fiber types on the market intended to address various design requirements and constraints. Table 1.1

Table 1.1—A compilation of mechanical properties of commonly used fibers in concrete materials*

Type of fiber	Equivalent diameter, mm	Specific gravity, kg/m ³	Tensile strength, MPa	Young's modulus, GPa	Ultimate elongation, %
Acrylic	0.02 to 0.35	1100	200 to 400	2	1.1
Asbestos	0.0015 to 0.02	3200	600 to 1000	83 to 138	1.0 to 2.0
Cotton	0.2 to 0.6	1500	400 to 700	4.8	3.0 to 10.0
Glass	0.005 to 0.15	2500	1000 to 2600	70 to 80	1.5 to 3.5
Graphite	0.008 to 0.009	1900	1000 to 2600	230 to 415	0.5 to 1.0
Aramid	0.010	1450	3500 to 3600	65 to 133	2.1 to 4.0
Nylon	0.02 to 0.40	1100	760 to 820	4.1	16 to 20
Polyester	0.02 to 0.40	1400	720 to 860	8.3	11 to 13
Polypropylene (PP)	0.02 to 1.00	900 to 950	200 to 760	3.5 to 15	5.0 to 25.0
Polyvinyl alcohol (PVA)	0.027 to 0.66	1300	900 to 1600	23 to 40	7 to 8
Carbon (standard)	—	1400	4000	230 to 240	1.4 to 1.8
Rayon	0.02 to 0.38	1500	400 to 600	6.9	10 to 25
Basalt	0.0106	2593	990	7.6	2.56
Polyethylene	0.025 to 1.0	960	200 to 300	5.0	3.0
Sisal	0.08 to 0.3	760 to 1100	228 to 800	11 to 27	2.1 to 4.2
Coconut	0.11 to 0.53	680 to 1020	108 to 250	2.5 to 4.5	14 to 41
Jute	0.1 to 0.2	1030	250 to 350	26 to 32	1.5 to 1.9
Steel	0.15 to 1.00	7840	345 to 3000	200	4 to 10

*Data from Nawy (1996), Kuraray (2007), Saechtling (1987), Sim et al. (2005), Toledo et al. (2000), and Balaguru and Shah (1992).

Notes: 1 mm = 0.039 in.; 1 kg/m³ = 0.06 lb/ft³; 1 MPa = 145 psi; 1 GPa = 1,450,000 psi.

summarizes the majority of materials used in fiber production and the typical range of mechanical properties for each fiber type.

1.2—Scope

The report is divided into three sections:

1. The physical properties of FRC;
2. The areas where concrete durability is affected by the addition of fibers; and
3. A series of applications where FRC use resulted in beneficial durability.

The various properties addressed and the wide selection available in formulating matrix systems allow performance-based specification of concrete materials using fibers to become a viable reality. The objective of this report is to provide a historical basis about current knowledge for concrete professionals to use in tailoring new, sustainable, and durable concrete mixtures.

CHAPTER 2—NOTATION, DEFINITIONS, AND ACRONYMS

2.1—Notation

A	=	aspect ratio
C	=	capacitance, farads
C_t	=	creep coefficient at time t
C_u	=	ultimate creep coefficient
d	=	fiber diameter, in. (mm)
E_f	=	modulus of elasticity of fibers, psi (MPa)
f	=	frequency of the AC, Hz
H_R	=	relative humidity
K_s	=	thermal conductivity, BTU h ⁻¹ ft ⁻¹ °F ⁻¹ (W·m ⁻¹ °C ⁻¹)
k	=	reaction rate of the corrosion responsible for strength loss
k_o	=	frequency factor of collisions between the reactants
l	=	fiber length, in. (mm)
Q_{cr}	=	correction factor to modify for nonstandard conditions
R	=	resistance, ohms
R_u	=	universal gas constant, lb ft/(°R·lb mol) (J/(mol·K))
s	=	normalized strength
T	=	temperature, °F (K)
t	=	time, days
V_f	=	volume fraction of fibers, in. ³ (mm ³)
X	=	X-capacity reactance, ohm
Z	=	impedance, ohms
ΔG_I	=	activation energy required for the reaction to take place, ft·lb/mol (KJ/mol)
ΔT_s	=	temperature difference through the thickness of the material with known thermal conductivity, °F (K)
ΔT_u	=	temperature difference through the thickness of the material with the unknown thermal conductivity, °F (K)
τ	=	shear stress, psi (MPa)
τ_o	=	Bingham yield stress, psi (MPa)
μ_o	=	Bingham plastic viscosity, lb·s/in. ² (N·s/m ²)
$\dot{\gamma}$	=	shear rate, in./s per in. (m/s per m)

2.2—Definitions

ACI provides a comprehensive list of definitions through an online resource, “ACI Concrete Terminology,” <http://terminology.concrete.org>. Definitions provided here complement that resource.

aspect ratio, fiber—the ratio of length to diameter of a fiber in which the diameter may be an equivalent diameter (see **fiber, equivalent diameter**).

fiber, equivalent diameter—diameter of a circle having an area equal to the average cross sectional area of a fiber.

tex—the mass in grams of 3280 ft (1 km) of strand or roving.

2.3—Acronyms

AASHTO	—	American Association of State Highway Transportation Officials
AC	—	alternating current
AC-IS	—	alternating current-impedance spectroscopy
AR	—	alkali-resistant
ARS	—	average residual strength
ASM International	—	The Materials Information Society
ASTM International	—	American Society for Testing and Materials
CAC	—	calcium aluminate cement
DC	—	direct current
DW	—	drawing-wire
FRC	—	fiber-reinforced concrete
FRCB	—	fiber-reinforced cement board
GFRC	—	glass fiber-reinforced concrete
HAC	—	high-alumina cement
HSC	—	high-strength concrete
IPC	—	inorganic phosphate cement
IS	—	impedance spectroscopy
NSC	—	normal-strength concrete
OPC	—	ordinary portland cement
PP	—	polypropylene
PVA	—	polyvinyl alcohol
SAC	—	sulfo-aluminate cement
SFRC	—	steel fiber-reinforced concrete

CHAPTER 3—PHYSICAL PROPERTIES OF FIBER-REINFORCED CONCRETE (FRC)

3.1—Creep

Creep is defined as a phenomenon in which strain in a solid increases with time while the stress producing the strain is kept constant. In more practical terms, creep is the increased strain or deformation of a structural element under a constant load. Depending on the construction material, structural design, and service conditions, creep can result in significant displacements in a structure. Severe creep strains can result in serviceability problems, stress redistribution, prestress loss, and even failure of structural elements. For some other structural elements such as bridge decks, however, severe creep strains can result in serviceability benefits.

3.1.1 Creep behavior of concrete—Concrete is known to deform considerably under constant loading and normal service conditions. Compressive creep strain in conventional concrete can be 1.30 to 4.15 times the initial elastic strain under standard conditions (ACI 209R; Troxell et al. 1958).

For certain non-standard conditions, such as low ambient relative humidity or high ambient temperature, creep strain can be even greater. Over time, these large creep strains result in shortened compression members and increased deflections in bending members.

The creep coefficient C_t is defined as the ratio of creep strain to initial elastic strain and is dependent upon the time t after application of stress. The method suggested in ACI 209R is most commonly used for predicting the creep behavior of concrete, using the following expression that is applicable for normal- to low-density concrete:

$$C_t = \frac{t^{0.6}}{10 + t^{0.6}} C_u Q_{cr} \quad (3-1)$$

where C_t is the creep coefficient at time t (days) after application of stress; C_u is the ultimate creep coefficient; and Q_{cr} is a correction factor to modify for nonstandard conditions. ACI Committee 209 intended for this expression to be used only if the sustained compressive stress is less than or equal to 50% of the concrete strength.

3.1.2 Creep behavior of fibers—Polymeric fibers are considered as viscoelastic materials and are more susceptible to creep than metallic and glass fibers. They tend to respond to short-time stresses in an elastic fashion. If a relatively high stress level is maintained for considerable time, however, polymeric materials will behave viscously and will creep, even exhibiting creep rupture (ASM International 1988). The strain to failure is usually high enough for stress redistribution and relaxation to take place, accommodating the deformation. Steel fibers do not exhibit creep behavior under normal service conditions at temperatures below approximately 700°F (370°C) (ASM International 1990).

3.1.3 Creep behavior of FRC—Given the low fiber dosages typically used in concrete (0.1 to 1% vol.), the presence of fibers (steel, synthetic, glass, cellulose) has a minimal, if any, impact on the creep behavior of concrete in compression. The flexural creep performance of conventionally reinforced concrete beams incorporating steel fiber-reinforced concrete (SFRC) showed smaller long-term deflections than the reinforced concrete beams without fibers (Tan et al. 1994).

The addition of fibers primarily benefits the post-crack behavior of concrete. The post-crack creep of FRC studied by Balaguru and Kurtz (2000) indicated that creep failure occurred in cracked micro-synthetic FRC for sustained stress levels. The definitions of macro- and micro-fibers can be found in ACI 544.3R. Micro-synthetic FRC could only sustain a small percentage of the post-crack stress. Creep of the fiber/matrix interface bond was an important aspect because most FRC mixtures are designed to fail in pullout mode rather than fiber-fracture mode.

The addition of macro- and micro-fibers (ACI 544.3R) primarily benefits the post-crack behavior of concrete. The post-crack creep of FRC studied by Balaguru and Kurtz (2000) indicated that creep failure occurred in cracked micro-polymeric FRC for sustained stress levels. Micro-polymeric FRC could only sustain a small percentage of the

post-crack stress. Creep of the fiber/matrix interface bond was an important aspect because most FRC mixtures are designed to fail in pullout mode rather than fiber-fracture mode.

The magnitude of load applied to a specific specimen during creep testing was based on the results of average residual strength (ARS) tests determined using ASTM C1399. Prior to creep testing, the beams were cracked by subjecting 4 x 4 x 14 in. (100 x 100 x 350 mm) beams to a deflection of 0.01 in. (0.2 mm). Specimens of the synthetic FRC mixture were creep tested at loads nominally equivalent to 20, 40, and 60% of the ARS value while the SFRC mixture was tested at loads nominally equivalent to 20, 40, 60, and 80% of the ARS value. The study concluded that, at similar loading levels, cracked synthetic FRC can be expected to experience creep coefficients twice that of SFRC.

Bernard (2004a) studied the creep of cracked FRC specimens and round panels based on ASTM C1550. High-modulus synthetic macrofibers, crimped low-modulus synthetic macro-fiber, and flat-end steel fiber were investigated for long-term creep behavior in cracked concrete specimens. Results indicated that the high-modulus synthetic macrofiber had creep behavior similar to the steel fiber, whereas the low-modulus synthetic macrofiber experienced much higher creep.

3.2—Shrinkage

Fibers can be added to concrete to reduce cracking potential due to shrinkage. Plastic shrinkage occurs during the early-age period when the strength of the paste is quite low, and drying shrinkage occurs due to volume change after the concrete hardens. If the shrinkage deformation is sufficiently restrained, the tensile stresses generated may be sufficiently high to cause cracking. The addition of synthetic or cellulose microfibers has been shown to increase the strength and strain capacity sufficiently during the very early ages (up to 12 hours) so that the potential for cracking under the tensile stresses generated by the shrinkage is minimized. Adding steel and macro-synthetic fibers has been shown to provide strength- and strain-carrying capacity after the concrete has hardened to the extent that the FRC resists and controls drying-shrinkage cracking. Understanding these principles is essential when designing durable structures.

Over the last century, several test methods have been used to evaluate the plastic and restrained shrinkage cracking behavior of mortar and concrete. While a wide range of tests are available, two tests have been standardized by ASTM to evaluate early-age cracking. The first test method, ASTM C1579, focuses on assessing the plastic shrinkage cracking behavior of concrete. This method uses a stress riser to simultaneously simulate the effects of evaporation, autogenous shrinkage, and settlement (Berke and Dalliare 1994). The stress riser, which focuses on a crack in a small region in the center of the sample, is intended to simulate conditions that occur above a reinforcing bar in practice (Qi and Weiss 2003; Qi et al. 2003; Banthia and Gupta 2006). The second test method, ASTM C1581, uses the restrained ring geometry to describe the restrained drying shrinkage cracking behavior of hardened concrete. Although the standardized testing procedure is relatively new, this testing approach has

been in use for cement pastes, mortars, and concretes for nearly a century. A review of developments in ring testing has been published (Radlinska et al. 2006) and the American Association of State Highway Transportation Officials (AASHTO) PP34 also recommends a provisional standard for performing a ring test.

3.2.1 Plastic shrinkage cracking—Numerous researchers have studied the effects of fibers on plastic shrinkage cracking behavior. A general observation is that a finer fiber is more effective in reducing the width of plastic shrinkage cracks than a coarse fiber (Qi and Weiss 2003; Banthia and Gupta 2006). Most fine-diameter microfibers with a high specific fiber surface area are particularly effective in reducing plastic shrinkage cracking.

Naaman et al. (2005) evaluated the effect of several fibers on the plastic shrinkage cracking characteristics of concrete including polypropylene (PP), PVA, Spectra, carbon, and steel, covering a wide range of properties. Prismatic concrete specimens freshly cast on top of a grooved, hard concrete substrate were subjected to adverse environmental conditions, namely, elevated temperature, low relative humidity, high volume, and airflow velocity. Testing parameters covered a range of fiber properties, including diameter, length, cross section, form, bond strength, and elastic modulus. Experimental results indicated that volume fraction and diameter of fiber reinforcement are the two most influential parameters in controlling plastic shrinkage cracking of concrete. For a given volume fraction of fibers, changing the fiber length or aspect ratio did not have a noticeable effect on plastic shrinkage cracking. Decreasing the fiber diameter or equivalently increasing the number of fibers crossing a unit area, however, did significantly improve the control of plastic shrinkage cracking. At a volume fraction of 0.2%, most fine-diameter polymeric fibers tested provided a reasonable control of plastic shrinkage cracking, reducing it to approximately 10% of control.

Najm and Balaguru (2002) studied the effect of polymeric fibers on the reduction of crack width caused by plastic and drying shrinkage. The variables included matrix composition, fiber geometry and aspect ratio, and fiber volume fraction, which ranged from 7.5 to 45 lb/yd³ (4.5 to 27 kg/m³). Fibers increased the strain capacity and reduced the crack width compared to control samples without reinforcement. An approximate fiber content of 15 lb/yd³ (9 kg/m³) resulted in a 60% reduction in crack width. In addition, polymeric macrofibers provided the same reduction in width of cracks as steel fibers at half the fiber volume fraction. Note that crack reductions include both plastic and drying shrinkage.

The shape of fiber effects were also studied by Ma et al. (2002) who evaluated different cross sections of PP microfibers. Test results showed that PP microfibers with circular cross section made by a drawing-wire (DW) technique had a more pronounced effect on the resistance to plastic shrinkage cracking than PP microfibers with rectangular cross section made by a fibrillated film technique. Polypropylene microfibers with a Y-shape cross section were slightly more effective in reducing plastic shrinkage cracking than the DW-PP fibers.

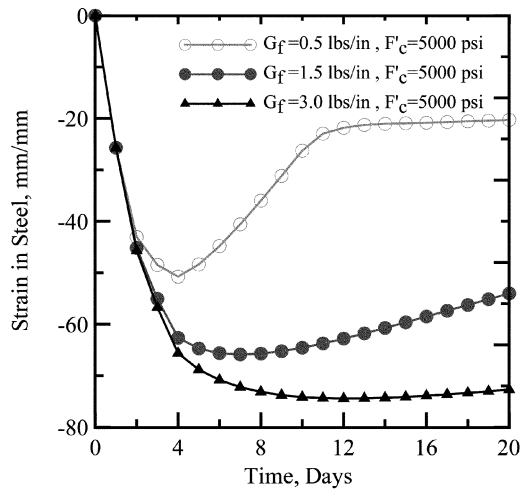
Banthia et al. (1996) and Banthia and Yan (2000) studied the plastic shrinkage cracking in polyolefin FRC using a substrate restraint type shrinkage test. Polyolefin fibers were generally effective in reducing the amount and size of shrinkage cracking, and their dimensions decisively influenced the results. Although crack widths were reduced from 0.005 in. (1 mm) in plain concrete to less than 0.002 in. (0.40 mm) with 0.7% by volume of the 2 in. (50 mm) long fibers, they were completely eliminated as the fiber length was reduced for similar levels of aspect ratio and volume fraction.

Qi et al. (2003) and Qi and Tianyou (2003) used image analysis to systematically characterize the size of the plastic shrinkage cracks that developed. They found it crucial to use a large set of measurements to obtain statistically reproducible results because of the large variation typical in crack width measurements. In addition to a reduction in the width of the plastic shrinkage cracks, fibrillated fibers were effective in reducing the rate of corrosion (Qi et al. 2006).

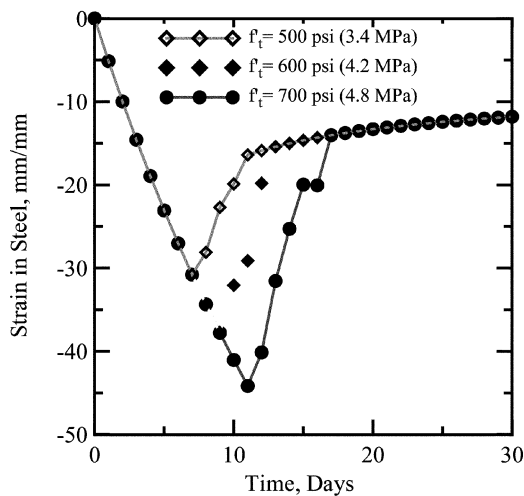
Wongtanakitcharoen and Naaman (2007) evaluated the plastic shrinkage cracking characteristics of concrete containing PP, polyvinyl alcohol (PVA), high-density polyethylene (HDPE), carbon, and metallic fibers during the first 24 hours after mixing. Testing parameters cover several fiber properties, including diameter, length, cross section, form, bond strength, and elastic modulus that were investigated under high temperature, low relative humidity, and high airflow volume and velocity. Results indicate that volume fraction and diameter of fiber reinforcement are the two most influential parameters in controlling plastic shrinkage cracking of concrete. For a given volume fraction of fibers, changing the fiber length or aspect ratio did not have a noticeable effect on plastic shrinkage cracking, whereas decreasing the fiber diameter significantly improved the plastic shrinkage cracking resistance. At a volume fraction of 0.2%, most fine-diameter fibers tested provided a reasonable control of plastic shrinkage cracking, reducing it to approximately 10% of control. Plain concrete mixtures shrink less at very early ages, presumably due to the bleed water that remains on the surface of the specimen for a longer time. Much of the shrinkage occurs before the mortar sets (as identified by the change in the slope of the shrinkage curve [Sant et al. 2006]).

3.2.2 Restrained shrinkage cracking—Bissonnette et al. (2000) conducted uniaxial restrained shrinkage tests and tensile tests on large-scale SFRC specimens with fiber contents ranging from 0 to 160 lb/yd³ (0 to 100 kg/m³). Multiple parallel microcracks altered the overall response of the SFRC beams in the hardened state.

Several recent studies have evaluated the influence of ring geometry and drying direction on the behavior of the restrained shrinkage test using the steel ring specimen (Swamy and Stavarides 1979; Hossain et al. 2003; Hossain and Weiss 2004). These studies demonstrated how the steel ring could be used to directly measure the residual stress that develops in the concrete as well as the stress relaxation that occurs. Mane et al. (2002) developed an experimental and analytical simulation algorithm to study the restrained shrinkage cracking in plain and fiber-reinforced concrete.



(a)

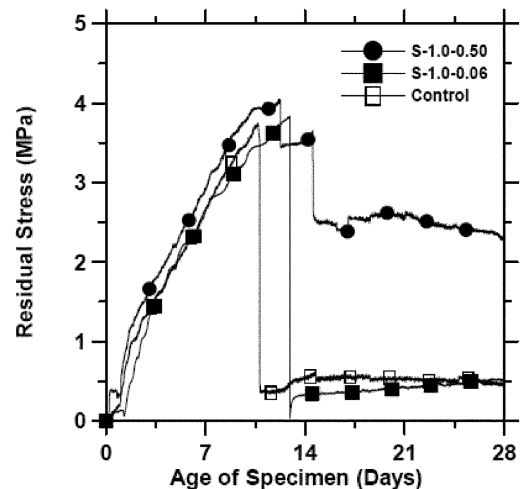


(b)

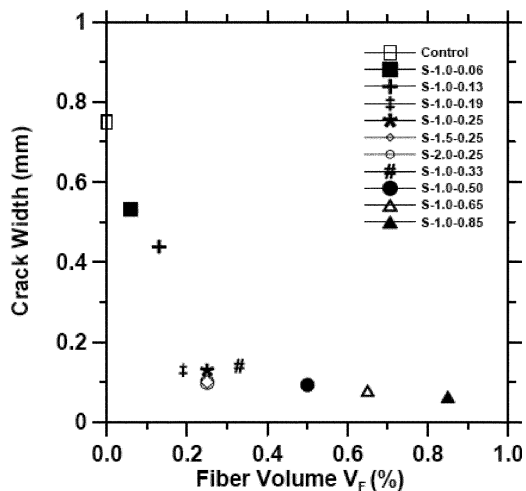
Fig. 3.1—Theoretical curve of restrained shrinkage test illustrating the effect of fracture energy and tensile strength of concrete (Mane et al. 2002): (a) effect of fracture energy of the FRC material representing an increase in fiber content on the stress relaxation in steel; and (b) effect of tensile strength of concrete with a proportional increase in fracture energy.

The effect of the geometry of the specimens, the humidity and shrinkage conditions, the restraint offered by the stiffness of the steel ring, and the concrete properties such as stiffness, shrinkage, and creep were studied using an analytical approach. The model is based on the stress analysis of a restrained concrete section and includes shrinkage, creep, aging, and microcracking. Using the theoretical models, it is possible to calibrate and interpret the experimental test results.

Figure 3.1(a) represents the theoretical curve of strain in the steel as a parametric study of the effect of fibers. The compressive stress builds up gradually in the steel, and as the concrete cracks from a tensile failure mode, there is a gradual relaxation and recovery of strain in steel. The strain in the steel does not decay as quickly as cracking takes place in the specimen, if the fracture energy is sufficiently high, which indicates the load transfer can take place. Figure 3.1(b)



(a)



(b)

Fig. 3.2—Influence of steel fibers volume on residual stress development and the influence of steel fiber volume on the crack width (Shah and Weiss 2006). (Notation: S-X-Y, X = fiber length, in.; Y = fiber volume, %.)

shows the effect of concrete strength on the cracking response. Only the first cracking point is affected as the tensile strength is increased. The first crack formation in the theoretical model is after 8 days, which is similar to the experimental results. Beyond the cracking of concrete, its creep properties in the post-peak region contribute to an increase in strain, causing further reduction of steel strain. Shah and Weiss (2006) demonstrated that, prior to cracking, the stresses that develop in plain concrete and in FRC are very similar (Fig. 3.2). They also developed an analytical procedure to describe how the strain that develops in the steel ring can be used to estimate the stress transferred across the crack and the size of the crack that develops in the ring; however, they also indicated that the small geometry of the ring may result in smaller crack widths and higher stress transfer than what may be expected in practice.

Voight et al. (2004) compared the performance of different fiber types, fiber blends, and welded-wire reinforcement in their ability to prevent and control drying-shrinkage

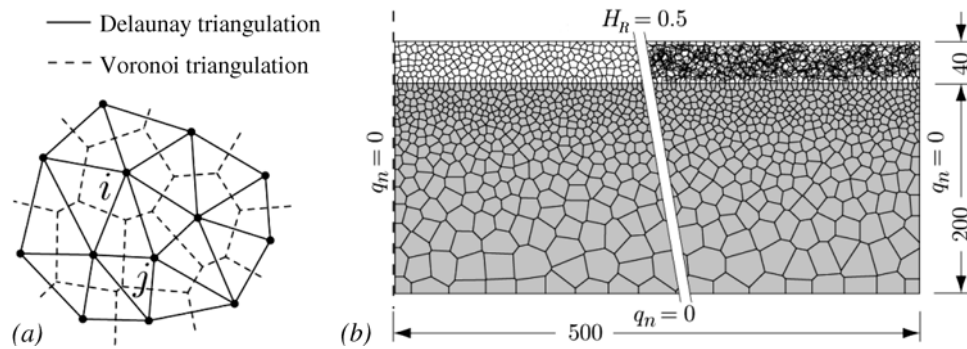


Fig. 3.3—(a) Element ij within irregular lattice; and (b) computational grid for simulating drying of an overlay system (fiber composite overlay shown on right side; dimensions are in mm) (Bolander and Berton 2004) (1 mm = 0.039 in.).

cracking. This program used the AASHTO PP34 ring shrinkage test to force cracks to occur in samples due to drying shrinkage. Several conclusions were made from the test. First, they concluded that fiber count is not a good indicator of controlling drying-shrinkage cracks. Approximately the same level of crack control is achieved by the same dosage of profiled 0.8 in. (20 mm), flat-end 1.2 in. (30 mm), and hooked-end 2 in. (50 mm) fibers, regardless of a significant difference in the fiber count. Second, a reasonable indicator of maximum crack width can be correlated to the value of the fiber volume V_f times the aspect ratio A . Therefore, fiber-reinforced concretes that have the same value for $V_f A$ provide a similar level of crack control. When volume or dosage rate is held constant, fibers with similar aspect ratios provide the same level of crack control.

Various models have been developed for predicting transverse cracking of concrete ring specimens due to drying shrinkage (Shah et al. 1998). These models have been developed based on nonlinear fracture mechanics. Using the measured material fracture parameters, the fracture resistance curve (R -curve) of the ring specimen is determined. Another model has been developed for a compatibility condition that equates the difference between measured free shrinkage and estimated creep with the maximum allowable tensile strain (Mane et al. 2002). Based on this condition, age at transverse cracking of the specimen subjected to restrained drying shrinkage can be predicted.

A model was proposed for predicting the shrinkage of SFRC from the composition of concrete mixture, strength, age when drying begins, conditions of environment, size and shape of structures, fiber volume ratio, and aspect ratio of the fiber (Young and Chern 1991). The model is based on the well-developed Bažant-Panula (BP) model for the shrinkage of plain concrete (Bažant et al. 1991; Bažant and Panula 1978). All important features of the BP prediction model, such as the diffusion-type size dependence of humidity effects and the square-root hyperbolic law for shrinkage, are adopted for SFRC.

Zhang and Li (2001) presented a model to predict the drying shrinkage performance of a fiber-reinforced cementitious composite. A free shrinkage expression is presented to show the influence of the matrix and fiber properties and fiber

orientation characteristics. Model results indicate that shrinkage of a fiber-reinforced cement-based composite is significantly influenced by the elastic modulus of the fiber and the matrix, as well as fiber length and diameter.

Bolander (2004) and Bolander and Berton (2004) have developed irregular lattice models of FRC in which the primary material phases—for example, fiber, matrix, and interfacial zone—are represented as separate entities (Fig. 3.3). The modeling of moisture diffusion, convective boundary conditions at exposed surfaces, and coupling of the stress and diffusion analyses are based on the works of Bažant and Najjar (1971) and Martinola and Wittmann (1995). Short fibers are explicitly modeled within the three-dimensional domain, directly accounting for length and orientation efficiency of each fiber and wall effects that can bias fiber orientations near the domain boundaries. Fiber distributions can be numerically generated, as has been done in cited works, or obtained from actual tests such as computed tomography. One objective is to simulate the effects of directional bias and non-uniformity of fiber distributions.

The lattice model has been used to study drying-shrinkage cracking in a fresh cement composite overlay on a mature concrete substrate and the role of fibers in restraining such cracking. Figure 3.3 shows a lattice discretization of the composite system. The lattice topology is based on the Delaunay triangulation of an irregular set of nodal points, whereas the dual Voronoi diagram serves to define the element properties. The overlay, substrate, and an interfacial layer are defined by their elasticity, hygral, and fracture properties. The upper face of the lattice model is exposed, via a convective boundary condition, to an environment with relative humidity $H_R = 0.5$, whereas the overlay and a portion of the substrate are assigned relative humidity $H_R = 1.0$. With exposure to the drying environment, the moisture diffusion analysis produces humidity gradients that lead to stress development in the overlay system. Without fiber reinforcement, fracture zones develop rather uniformly along the top of the overlay prior to 20 days of exposure to drying. With shrinkage due to additional drying, localization occurs as characterized by several of the cracks continuing to open while neighboring cracks unload. A maximum crack opening of 0.014 in. (0.29 mm) occurs after 110 days of

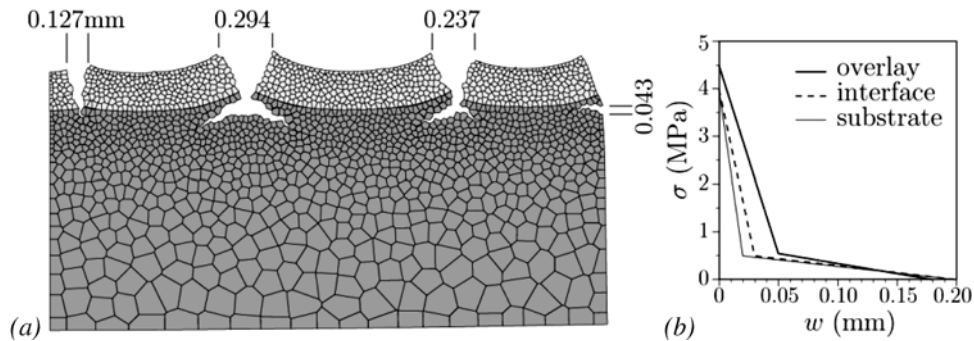


Fig. 3.4—Unreinforced overlay: (a) damage pattern after 110 days of exposure to drying environment; and (b) stress versus crack opening relations for system components (Bolander and Berton 2004). (Note: 1 mm = 0.039 in.; 1 MPa = 145 psi.)

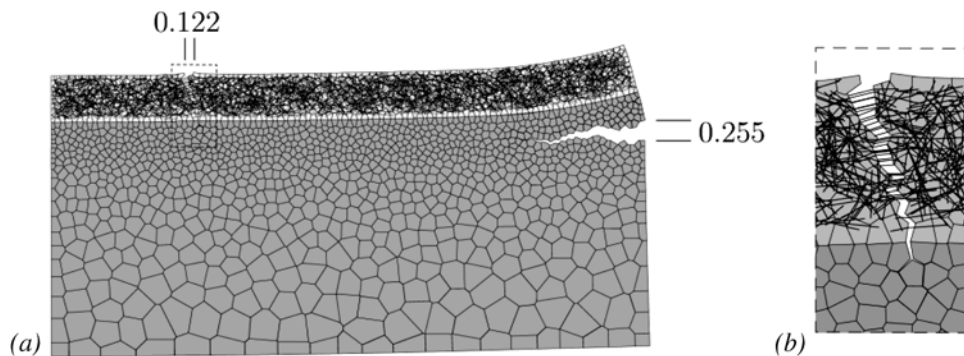


Fig. 3.5—Fiber-reinforced overlay: (a) damage pattern after 110 days of exposure to drying environment; and (b) fibers bridging a crack in the overlay (dimensions in mm) (Bolander and Berton 2004). (Note: 1 mm = 0.039 in.)

drying (Fig. 3.4(a)). The pattern of cracks in the overlay, as well as the tendency for vertical overlay cracks to turn and run laterally, are in good general agreement with the results presented by Martinola and Wittmann (1995). When PVA fibers (diameter = 0.005 in. [0.12 mm], length = 1.5 in. [39 mm], $E_f = 6 \times 10^6$ psi [42.8 GPa], $V_f = 2\%$) are introduced into the overlay material, diffuse microcracking still occurs along the top of the overlay, but only one smaller crack runs through the thickness of the overlay. The fibers restrict the opening of this crack to 0.005 in. (0.12 mm) after 110 days of drying, and the undesirable lateral branching of cracks is also arrested (Fig. 3.5). The fibers restrict the opening of this crack to 0.0005 in. (0.12 mm) in the overlay after 110 days of drying and the undesirable lateral branching of cracks is also arrested (Fig. 3.5). Due to restraining the width of cracks by fibers in the overlay, relief is achieved by horizontal cracks developing in the substrate, starting from the edge of the overlay/substrate system.

3.3—Permeability and diffusion

Concrete is susceptible to degradation through corrosion, alkali-silica reaction, sulfate attack, freezing-and-thawing damage, and other mechanisms that result from the ingress of water. Concrete durability is, therefore, intimately related to the rate at which water is able to penetrate it (water permeability). Fiber-reinforced concrete has been used in applications where water-tightness is desired, such as tunnel linings and

liquid storage tanks (Bentur and Mindess 1990; Mindess et al. 2003). The permeability of dense concrete, such as that with a water-to-cement ratio less than approximately 0.45, is nearly negligible in an uncracked condition. Permeability, however, is vastly increased by the introduction of cracks and increases with crack width (Ludirdja et al. 1989; Wang et al. 1997). Fiber reinforcement influences the way cracks develop in concrete and may impart improved crack growth resistance, increased surface roughness of individual cracks, and a greater likelihood for crack branching and multiple crack development. Due to this, fiber reinforcement may be used to significantly reduce the permeability of cracked concrete.

A number of studies have been conducted to investigate the relationship between FRC and water permeability. Tsukamoto and Wörner (1991) studied the permeability of cracked FRC using uniaxial tension tests of notched-rectangular prisms. A reduction in flow rate through the reinforced specimen was observed versus an unreinforced specimen deformed by the same amount. Aldea et al. (2000) evaluated the effect of fiber length and crack width (0 to 0.012 in. [0 to 300 μ m]) on water permeability and resistance to penetration of chloride ions of PVA fiber-reinforced mortars at an unloaded state, in which a crack had been induced using a tensile splitting configuration. It was observed that when fibers initiated crack branching, a lower water permeability resulted. Water permeability was significantly more sensitive

than resistance to chloride ion penetration within the crack range studied. Rapoport et al. (2002) and Aldea et al. (2001) studied the effect of steel fiber volumes (0, 0.5, and 1%) and crack width (0 to 0.012 in. [0 to 300 μm]) on low-pressure water permeability of steel fiber-reinforced normal-strength concrete (NSC) at an unloaded (relaxed) and loaded state, respectively, in which cracks were induced by a feedback-controlled splitting tension test. In conclusion, the steel fibers decreased the permeability of specimens for cracks larger than 0.004 in. (100 μm), whereas below 0.004 in. (100 μm), they do not seem to affect the permeability of concrete. Lawler et al. (2002) evaluated the relationship between multiple cracking, fiber reinforcement, and permeability by measuring the water permeability of fiber-reinforced mortars during uniaxial tensile tests on unnotched specimens. This method of testing permitted distributed multiple cracks to develop, and as a result, this study found that a significant reduction in water flow rate at a given displacement is possible with fiber reinforcement, depending on the fiber type and volume. The flow rate versus uniaxial tensile displacement for mortar containing various levels of reinforcement is shown in Fig. 3.6.

To directly investigate the effects fibers have on the durability of concrete structures, Sanjuán et al. (1997) included PP fibers in the cover over conventional steel reinforcement. Mortar was cast around steel bars in specimens that were then exposed to restrained shrinkage conditions immediately after casting. After curing, the specimens were ponded with a chloride ion-rich solution while the rate of corrosion in the steel was monitored. Fiber-reinforced matrixes cracked less and demonstrated lower corrosion rates showing the direct impact of fibers on permeability-related deterioration mechanisms.

Concrete materials that contain cracks of approximately 0.004 in. (100 μm) in width show a substantial increase in water permeability both for plain concrete (Wang et al. 1997) and FRC (Aldea et al. 2001; Lawler et al. 2002). This suggests a threshold level for use as a design criterion below which crack widths should be maintained to maximize the durability of concrete structures. While further work is required to confirm a relationship between crack width and concrete durability, one potential means to achieve such a criterion is with fibers. Further discussion about this can be found in Section 3.5 of ACI 224.2R regarding the relationship between crack width and serviceability.

Gas permeability is another method that is commonly used to evaluate durability characteristics of concrete. Picandet et al. (2001) examined the effect of axial compressive loading on the permeability of three different types of concrete: ordinary, high-strength, and steel fiber-reinforced concrete. Monotonic and cyclic loads were applied on 8 x 4 in. (200 x 100 mm) diameter specimens using stress levels between 60% and 90% of the ultimate strength. At the end of the loading phase, a disc was extracted from the middle part of the cylinders, and four different gas permeability tests were conducted during the drying procedure. A relationship between mechanical damage indicators and the increase in permeability was proposed.

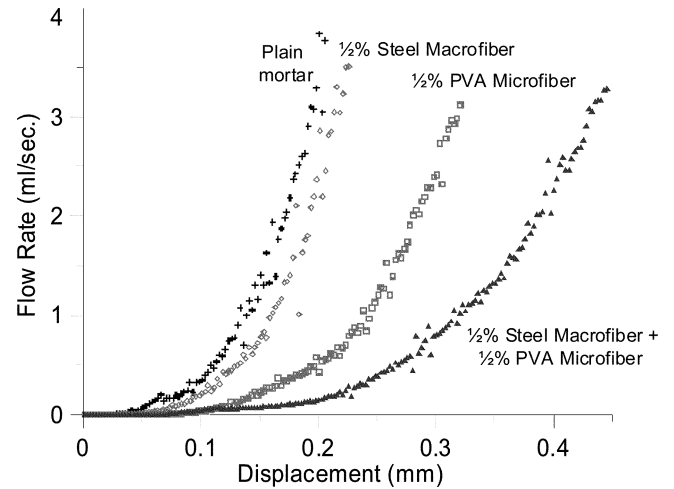


Fig. 3.6—Flow rate versus uniaxial tensile displacement for mortar specimens containing various levels of reinforcement (Lawler et al. 2002).

3.4—Rheology

The characteristics of FRC in a fresh state can be described using rheological parameters that characterize flow, or deformation, under stress. These parameters enable workability, flow, pumping ability, placement, compaction, and finishing characteristics to be quantitatively monitored and used during the construction phase.

A variety of test methods exist to describe the rheological properties. Tattersall (1991) classified three test categories: qualitative, quantitative-empirical, and quantitative-fundamental. Qualitative tests are subjective. Quantitative-empirical methods give limited information about flow behavior under certain conditions and include the slump test, vebe flow time, and inverted cone test. Quantitative-fundamental tests measure true material flow properties. These properties are typically evaluated using rheometers, which measure a material's response to shear. While measuring the fundamental flow properties of FRC is preferred, it is difficult with conventional rheometers, which are only suited for small sample sizes and highly flowable materials.

3.4.1 Empirical rheology—Researchers have studied the influence of fibers on the rheology of FRC for over 25 years. A number of parameters affect flow behavior, including the physical characteristics, fiber content, matrix properties, aggregate content, and the processing methods. Two of the most prominent factors affecting flow are the aspect ratio (fiber length/diameter) and the volume fraction of fibers. The combined effect of these two parameters is defined as “reinforcement index,” or “fiber factor” as $(l/d) \times V_f$, where l = fiber length, d = fiber diameter, and V_f = volume fraction of fibers (Hughes and Fattuhi 1976).

Early work relied on quantitative empirical tests to evaluate the flow behavior of SFRC. Researchers found that the key factors affecting rheology were the fiber volume, aspect ratio, type, and geometry. Hughes and Fattuhi (1976) showed that workability decreases proportionately with $(l/d)^{1/2} \times V_f$. Swamy and Mangat (1974), Mangat and Swamy (1974), and Bayasi and Soroushian (1992) showed

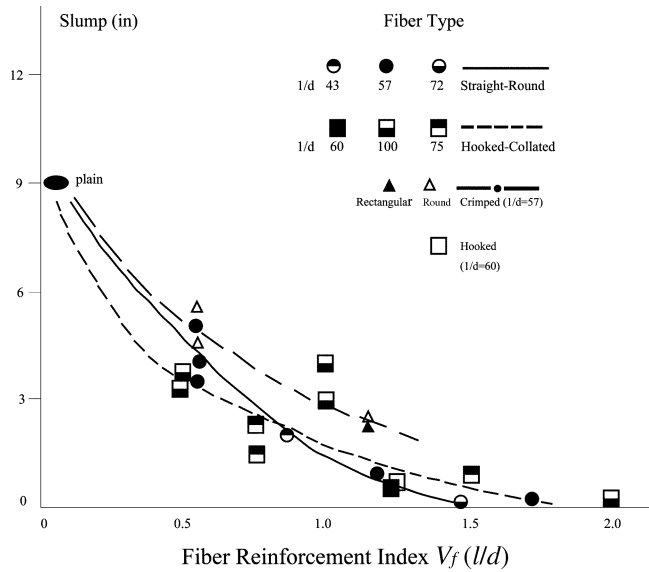


Fig. 3.7—Effect of fiber reinforcement index and type on slump (Bayasi and Soroushian 1992).

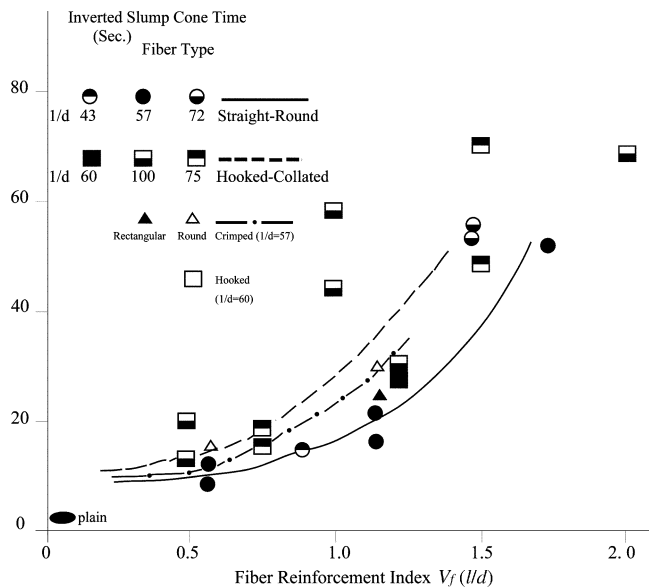


Fig. 3.8—Effect of fiber reinforcement index and type on inverted slump cone time (Bayasi and Soroushian 1992).

that the fresh-state properties worsen as the fiber reinforcement index increases, and that the rate of change is directly related to the fiber type. Varying steel fiber geometries were evaluated, including straight-round, hooked-end, duoform, and crimped (deformed continuously along the length) fibers. Generally, crimped fibers were shown to have slightly higher workability than the other geometries. Figures 3.7 and 3.8 present results from Bayasi and Soroushian (1992) that show the effects of fiber reinforcement index on the slump and inverted cone time, respectively.

To improve the fresh state properties of SFRC, collated fibers were developed. These fibers have deformed ends that are adhered together using water-reactive glue. Thus, as the fibers are first added to the mixture they have a lower aspect

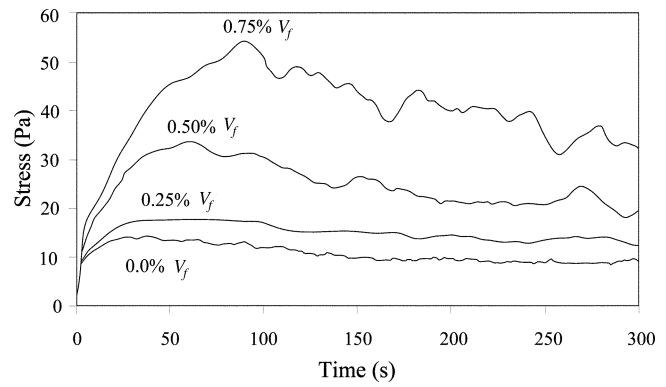


Fig. 3.9—Effect of cellulose fiber content on the yield stress of neat paste (w/c = 0.50) measured with a commercial rheometer using the vane configuration (Rapoport and Shah 2005).

ratio, facilitating better mixing. Ramakrishnan et al. (1980) and colleagues found that the dispersion of hooked-end fibers improved with the use of the collated fibers. Giaccio et al. (1986) studied the effect of mixing time on the separation of individual fibers from bundles, which is needed to get the full mechanical advantage of the fibers. Research indicated that shorter mixing times were better for workability, but were not sufficient for separating the fibers.

3.4.2 Quantitative rheology—Recently, researchers have attempted to obtain flow properties of FRC by using rheometers. Two categories of rheometers are considered: commercially available and custom designed. Commercially available rheometers were originally developed for polymer systems and allow for different geometries such as the parallel plate, coaxial cylinder, and vane configurations used as interchangeable fixtures of a single machine. Small sample sizes and a low torque capacity, however, limit the testing to relatively fluid cement paste and mortar systems, typically without fiber reinforcement. In response to these limitations, a number of research grade rheometers have been developed for highly fluid concrete materials. Custom designed rheometers include mixer-type setups (Beaupre 1994; Struble et al. 2001; Tattersall and Bloomer 1979), coaxial cylinder configurations (Coussot 1993; Wallevik and Gjrv 1990), and parallel plate geometries (Hu et al. 1996), as well as the rheometer developed at the University of Illinois at Urbana-Champaign (Struble et al. 2001).

A number of different models exist to describe the rheological characteristics of cementitious systems. The most commonly used model is the Bingham model, which is given by

$$\tau = \tau_o + \mu_o \dot{\gamma} \tag{3-2}$$

where τ_o is the Bingham yield stress describing the stress needed to initiate flow; μ_o is the Bingham plastic viscosity, which is the resistance of the material to flow; and τ and $\dot{\gamma}$ are the shear stress and shear rate, respectively. Malek and Roy (1991) reviewed other models, including the Herschel-Bulkley, Vom Berg, Casson, Ellis, Eyring, Robertson-Stiff,

Williamson, Sisko, and Atzeni. Flow curves obtained with rheometers are used to fit the data to these models.

Rapoport and Shah (2005) used a commercial scale rheometer to describe the rheology of cellulose fiber-reinforced cement paste and mortar. The peak yield stress of the mixtures was determined using the vane geometry. Yield stress curves are shown in Fig. 3.9 and indicate that the yield stress increases as the amount of cellulose fibers increases. Because a commercial rheometer was used, the viscosity of the fiber-reinforced pastes and mortars could not be obtained for these stiff mixtures. The authors, therefore, evaluated the viscosity of the matrix only and used this information to describe the flow behavior of the entire system.

Bui et al. (2003) evaluated the effects of steel and PP fibers on the flow behavior of highly fluid mortar using a concentric cylinder rheometer (Wallevik and Gjørv 1990). The Bingham parameters were used to describe flow. They found that the rheology of the mortar was influenced by fiber content, the ratio between the fiber volume fraction and maximum packing density of fibers, the radius and length of the fibers, and the properties of the matrix.

A custom-designed and built parallel plate rheometer was developed by Kuder and coworkers to evaluate the rheology of stiff fiber-reinforced cement pastes and mortars (Kuder et al. 2004). The effect of steel fiber volume on the rheological parameters was studied. Bingham yield stress and viscosity decreased with increased fiber content until a critical volume fraction was reached. This trend was explained by a coupling effect between the structural breakdown of the cement paste, which occurs at low fiber volumes, and the mechanical interlocking of the fibers, which occurs at higher volume fractions. These results demonstrate the potential differences in rheological trends when stiffer cementitious systems are investigated.

3.4.3 Relating rheology, fiber dispersion, and mechanical performance—Fiber dispersion is known to affect the mechanical performance of FRC. Because fiber dispersion is influenced by fresh-state properties, researchers have begun to link rheology, fiber dispersion, and mechanical performance. Ferrara (2003) and Özyurt et al. (2006a) used viscosity-modifying admixtures to improve fiber distribution in steel SFRC. The improvement in fiber distribution also led to an enhancement of mechanical properties.

While the effects of fibers on the rheology of the FRC have been studied for many years, our understanding of these systems is limited. The development of new rheometers suitable for testing these systems allows for fundamental flow properties to be identified. With an improved understanding of how fibers affect rheology, FRC can be designed so they are easy to work with during the fresh state to achieve the desired hardened-state properties.

3.5—Electrical properties

Many research studies have concentrated on using electrical methods as a means of characterizing concrete and developing potential applications for new materials, nondestructive testing, or diagnostic equipment (McCarter 1996). Various test results support the concept that the electrical conductivity of concrete is essentially electrolytic by ion transport through

the interconnected pore network. The electrical resistance of concrete ranges by several orders of magnitude between a moist-cured condition and oven-dried (Hammond and Robson 1955). Concrete is thought to behave as a parallel circuit of a capacitor and resistor. Its impedance to an alternating current (AC) is

$$\frac{1}{Z^2} = \frac{1}{X^2} + \frac{1}{R^2} \quad (3-3)$$

where Z = impedance, ohms; R = resistance, ohms; $X = 1/fC$ = capacitive reactance, ohms; f = frequency of the AC, Hz; and C = capacitance, farads.

For an AC, the capacitive reactance is always much greater than the resistance because the capacitance is small, which implies that the overall impedance using AC power is nearly equal to the direct current (DC) resistance. Following the introduction of a technique known as alternating current-impedance spectroscopy (AC-IS), researchers have concentrated on the use of the equivalent circuit modeling for the microstructural characterization of concrete at various stages of hydration (Christensen et al. 1994; McCarter and Brosseau 1990; Gu et al. 1992a,b).

Carbon or steel fibers can be added to a cement matrix at a high volume fraction of 0.5 to 3% (in further examples cited) to increase the conductivity of the composite. The mechanical status of the cement composite can affect the electrical properties (DC resistance and AC impedance) of the composite. Measurements of these electrical properties can be used as an indirect, nondestructive test for cement composites, making possible the detection of damage with only the use of simple and inexpensive electrical equipment, leading to the development of a smart material. This capability is based on the assumption that the volume electrical resistivity of the composite depends on crack generation and propagation under stress. The combined use of IS and computer simulation showed that the presence of highly conductive, oriented fibers in a relatively poor-conducting matrix induces changes in the impedance spectrum that can be quantitatively associated with fiber length, orientation, and volume fraction. The main effect was the resistance at DC or low-frequency AC depended almost entirely on the matrix, while the resistance at high frequencies depended almost solely on the fiber properties and geometry. Using this frequency-dependent “separation” of fiber and matrix behavior, the crack propagation process of FRC has been studied (Torrents et al. 2001).

Torrents et al. (2000) investigated the correlation between electrical (DC and AC) and mechanical properties of cement composites reinforced with conductive carbon fibers. The tensile and impedance behavior of extruded and notched composites with fiber volume fractions of 0.5% and 3% were examined. Mechanical loads and an electrical field were applied, and crack growth during loading was analyzed by digital image correlation (DIC). Impedance Spectroscopy measurements were made under loaded and unloaded conditions to address the effect of specimen geometry, the manufacturing process, and the effect of fiber volume fraction.

Using these IS measurements, along with numerical computations, the bridging area of the fibers was extracted quantitatively from the tensile measurements. A good correlation between the electrical and mechanical properties was found when a sudden growth of the crack was observed; a dramatic change was also noticed in the impedance values.

Impedance measurements have been used along with the conventional mechanical tests for assessing damage under load in composites reinforced with conductive fibers. Taking advantage of the special frequency-dependent electrical properties of conductive FRC, impedance values measured during the fracture process were used to distinguish and calculate three different areas at the crack front: uncracked, bridging, and open areas. The bridging area is the zone where fibers bridge the propagating crack. A greater bridging area was found for the 0.5% fiber composite than for the 3% fiber composite, due to differences in the final length of the carbon fibers in both composites. The high content of fibers in the 3% fiber system increased the stiffness of the fresh mixture, leading to higher forces during mixing and extruding, which resulted in increased fiber breakage and shorter final length, as confirmed by optical microscopy (Peled et al. 2001).

The addition of carbon fibers to portland cement-based concrete decreases the bulk electrical resistivity. Reza et al. (2001, 2003, 2004) measured the electrical resistivity of carbon FRC specimens as a function of curing time. The dependence of this electrical resistivity on the water-cementitious material ratio (w/cm), sand-cement ratio, volume fraction of carbon fibers in the mixture, and the length of fibers was determined. Results indicate incorporation of carbon fibers in amounts as low as 0.5% by volume significantly decreased the bulk electrical resistivity of mortar. The four-ring electrode configuration was an effective method for measuring the volume electrical resistivity of concrete samples. The w/cm did not significantly affect the electrical resistivity in the presence of carbon fibers.

Alternating current power is preferred for measuring the electrical properties of FRC. Direct current power exhibits a voltage across the inner ring electrodes for several minutes after the power is turned off creating a polarization potential that reduces the voltage drop across the ring electrodes. A discussion of the polarization potential can be found in Monfore (1968) and Banthia et al. (1992), who both made electrical resistivity measurements of combinations of carbon and steel fiber-reinforced mortars. Niemuth (2004) used electrical impedance to detect and image cracking in concrete elements. The state of stress is related specifically to the electrical conductivity or volume resistivity of carbon fiber-reinforced mortar (CFRM). By applying an AC current in the frequency range of 20 Hz to 1 MHz, Nyquist plots were made of the imaginary part of the impedance, reactance, versus the real part of the impedance, resistance (Torrents et al. 2000).

Owing to a unique frequency-dependent behavior of conductive fibers, Woo et al. (2005) employed AC-IS to monitor various dispersion issues in steel fiber-reinforced, cement-based materials. First, AC-IS was used on model-scale specimens to understand the ability of the method for

monitoring various dispersion issues such as fiber clumping, fiber orientation, and segregation. Mathematical expressions based on an intrinsic conductivity approach were used to evaluate characteristics of fiber dispersion, and very good results were obtained (Douglas and Garboczi 1995). Next, AC-IS was compared with a conventional time- and labor-intensive image analysis (Özyurt et al. 2006a), and fiber clumping and fiber orientation were measured using AC-IS and image analysis. The results of the two methods were found to match well in experimental uncertainty. Later, model studies on small-scale specimens were extended to large-scale specimens. Fiber orientation in an industrial-scale beam was evaluated using AC-IS and image analysis (Özyurt et al. 2004), and both methods gave similar results. Finally, fiber segregation in cylindrical specimens was studied by obtaining AC-IS measurements along the height of cylinders (Özyurt et al. 2007). The results were successfully used to relate fresh state properties to fiber segregation. Woo et al. (2005) recently showed that measurements related to fiber dispersion monitoring can be extended to fresh-state fiber-reinforced materials. By using AC-IS with another electrical measurement technique (time domain reflectometry), they determined the parameters necessary for fiber dispersion analysis at early times (Özyurt et al. 2006b).

Current research activity on the use of AC-IS for non-destructive monitoring of fiber dispersion deals with the assessment of its applicability to real size structural elements, with the objective of implementing such a technique into quality control procedures at the industrial scale. The uniformity of dispersion as well as issues related to the orientation of fibers play a major role in the promotion of SFRC in full load-bearing structural elements. Within the broadest range of foreseeable applications, attention has been focused on thin web roof elements.

3.6—Thermal conductivity

Both transient (unsteady heat flow) and steady-state heat flow are used for measuring the thermal conductivity of materials. The transient heat flow or “probe” procedure is well suited for homogeneous materials, while the steady-state heat flow procedure is better suited to nonhomogeneous materials such as mortar and concrete. In the steady-state procedure, a linear heat flow is created and the thermal temperature gradient is measured.

Cook and Uher (1973) used blocks of FRC with a copper plug and a resistor inserted in a hole on the top surface and the bottom surface in contact with a water-cooled, copper heat sink. The fiber concrete blocks were 3 x 3 x 6 in. (75 x 75 x 150 mm) and made of a mortar or concrete mixture containing 0.0, 0.5, 1.0, 2.0, 4.0, and 8.0% volume of copper fibers or steel fibers, 0.003 in. (0.8 mm) in diameter and 1 in. (25 mm) long. Thermal conductivity measurements were compared with a mathematical model developed by Lakkad et al. (1972) that provided upper and lower bounds on the thermal conductivity. The thermal conductivity of the plain mortar was 0.862 W/m °C and that of the concrete was 1.530 W/m °C. Morel (1970) investigated concrete mixtures with 0.0, 0.5, 1.0, and 1.5% volume of steel fibers with two

Table 3.1—Thermal conductivity measurements of fiber-reinforced mortar by Morel (1970)

Fiber volume percent and fiber shape	Thermal conductivity, W/m°C
0.0	2.75
0.5 flat	2.67
1.0 flat	2.80
1.5 flat	3.03
0.5 crimped	3.03
1.0 crimped	2.74
1.5 crimped	2.84

Note: $1 \text{ W}\cdot\text{m}^{-1} \text{ }^\circ\text{C}^{-1} = 0.578 \text{ BTU h}^{-1}\text{ft}^{-1}\text{ }^\circ\text{F}^{-1}$.

different geometric shapes: flat and crimped. The concrete was a mortar with a w/cm of 0.60 and sand-cement ratio of 2.50. The thermal conductivity of the SFRC can be calculated by the following equation for steady-state conditions

$$K_u = K_s \frac{\Delta T_s}{\Delta T_u} \quad (3-4)$$

where K_u = unknown thermal conductivity; K_s = known thermal conductivity; ΔT_s = temperature difference through the thickness of the material with known thermal conductivity;

and ΔT_u = temperature difference through the thickness of the material with the unknown thermal conductivity.

Any free moisture will change the thermal conductivity during the test; it will take several hours before the stack reaches steady-state conditions. Prior to testing, it is recommended to oven-dry the FRC at 302°F (150°C) until a constant weight is achieved (Thompson 1968). The thermal conductivity measurements in Table 3.1 are based on the average of three stacks of each fiber volume percentage for the two geometric fiber shapes in a mortar matrix.

The main difficulty associated with the steady heat flow procedure to measure thermal conductivity of concrete is moisture migration (Thompson 1968). A 10% increase in moisture can result in a 50% or more increase in thermal conductivity. The increase depends on the concrete porosity (diffusion coefficient) and water movement. The thermal conductivity of concrete depends on the aggregate type and ranges from limestone (3.1), sandstone (3.9), granite (3.1), and basalt (1.4) W/m °C that results in an approximate range of 1.4 to 3.9 W/m °C (Troxell et al. 1968).

The thermal conductivity data recorded by Cook and Uher (1973) and by Morel (1970) indicate that, although there are slight increases in thermal conductivity for paste and mortar containing steel fibers, the increase is less than the effect of coarse aggregate normally found in concrete.

To purchase a complete copy of ACI 544.5R-10,
please visit the [ACI Bookstore](#).